行政院國家科學委員會專題研究計畫 期中進度報告

新的形狀記憶合金之研究--新的鐵基形狀記憶合金之研究(2/3)

期中進度報告(精簡版)

計 畫 類 別 ： 整合型
計 畫 編 號 ： NSC 95-2221-E-002-165-
執 行 期 間 ： 95 年 08 月 01 日至 96 年 07 月 31 日
執 行 單 位 ： 國立臺灣大學材料科學與工程學系暨研究所

計 畫 主 持 人 ： 林新智
共 同 主 持 人 ： 林昆明

報 告 附 件 ： 出席國際會議研究心得報告及發表論文

處 理 方 式 ： 期中報告不提供公開查詢

中 華 民 國 96 年 05 月 30 日

行政院國家科學委員會補助專題研究計畫□ 成 果 報 告
■期中進度報告

新的鐵基形狀記憶合金之研究(2/3)

計畫類別：□ 個別型計畫　　■ 整合型計畫
計畫編號：NSC 95-2221-E-002 -165
執行期間：95 年 08 月 01 日至 96 年 07 月 31 日

計畫主持人：林新智　教授

共同主持人：林昆明　教授

計畫參與人員：王姿蘋、吳維仁

成果報告類型(依經費核定清單規定繳交)：■精簡報告　□完整報告

本成果報告包括以下應繳交之附件：
□赴國外出差或研習心得報告一份
□赴大陸地區出差或研習心得報告一份
■出席國際學術會議心得報告及發表之論文各一份
□國際合作研究計畫國外研究報告書一份

處理方式：除產學合作研究計畫、提升產業技術及人才培育研究計畫、列管計畫及下列情形者外，得立即公開查詢
□涉及專利或其他智慧財產權，□一年□二年後可公開查詢

執行單位：臺灣大學材料科學與工程學系暨研究所

中　華　民　國　96　年　05　月　25　日

中文摘要

本研究應用VAR熔煉技術配製不同成分之Fe-Mn-Si-Cr--IA (interstitial-site atom)形狀記憶合金，包括Fe-Mn-Si-Cr-C與Fe-Mn-Si-Cr-N等，並探討合金顯微組織、形狀回復特性與相變態溫度等。實驗結果顯示：在Fe-Mn-Si-Cr形狀記憶合金中添加間隙型元素C及N，因可強化沃斯田體相，進而有效提昇其形狀記憶效應。C及N元素添加量約為0.05~0.2wt%時可呈現最佳記憶效應。Fe-Mn-Si-Cr--IA形狀記憶合金於熱輥壓狀態，因合金內部存有過多差排，其記憶效應未達60%，經過500~700℃之熱處理後，熱輥壓殘留之內應力逐漸消除並產生再結晶現象，因而大幅提高其形狀回復率至90~92%。但當熱處理溫度高於800℃時，晶粒快速成長，且由於晶界相析出與合金內部存有較多的ε麻田散鐵相，因而形狀回復率降低許多。

關鍵詞：Fe-Mn-Si-Cr記憶合金、麻田散體相變態、間隙型元素、形狀記憶效應

Abstract

The Fe-Mn-Si-Cr--IA (interstitial-site atom) shape memory alloys, including Fe-Mn-Si-Cr-C and Fe-Mn-Si-Cr-N were prepared by vacuum arc re-melting (VAR) technique. Their microstructure, shape memory effect and transformation temperature were investigated. Experimental results show that the shape memory effect of Fe-Mn-Si-Cr alloys can be effectively improved by slight addition of carbon and nitrogen elements, due to the strengthening of Austenite phase. The Fe-Mn-Si-Cr alloys with 0.05~0.2wt% addition of carbon and nitrogen will exhibit the best shape memory effect. The as hot-rolled Fe-Mn-Si-Cr--IA shape memory alloys have worse shape memory effect, lower than 60%, because of the existence of many residual dislocations. The heat treatment at 500~700℃ will reduce gradually the residual internal stress and occur the phenomenon of recrystallization. These features can increase their shape recovery to 90~92%. However, if the heat-treating temperature is higher than 800℃, the shape recovery will reduce significantly due to the grain growth, precipitation of grain-boundary phase and the existence of more ε martensite within the matrix.

keywords： Fe-Mn-Si-Cr shape memory alloys, martensitic transformation, interstitial-site atom, shape memory effect

一、緣由與目的

形狀記憶合金以TiNi基記憶合金【1, 2】的使用最為廣泛，它具有較佳的形狀記憶能力、耐蝕性及生物相容性等特性，但其價格昂貴使得應用上有所限制。與TiNi基合金相比，鐵基形狀記憶合金具有強度高、易加工、價格低廉等優點【3】，故在工業上具有極大的應用潛力與市場競爭力。

鐵基形狀記憶合金的應用，最具潛力的是製成套筒元件—即管接頭，用於水電管路、輸油管、瓦斯管線等之接合。鐵基記憶合金中，又以Fe-Mn-Si基合金最為重要。然而，相較於TiNi記憶合金，Fe-Mn-Si基合金形狀記憶效應較差，造成合金在應用上的限制。因此，如何提昇Fe-Mn-Si基合金之形狀記憶能力是相當重要的研究主題。

改善鐵基記憶合金形狀回復率之方法，主要有下列幾種：(1)添加合金元素【4, 5】，(2)晶粒細化等基底強化機制，及(3)熱機訓練等【6-8】。文獻【3, 9】中曾指出，添加間隙型元素C及N可提昇Fe-Mn-Si基合金之形狀記憶效應，但對於C、N元素添加之實際效應以及這些元素對於合金顯微結構之影響，則尚未有明確之分析與探討，故本研究之目的為添加適量之C、N元素於Fe-Mn-Si-Cr合金中，藉以提升其形狀記憶效應，並探討添加C、N元素後，合金顯微組織、相變態行為等之變化，並藉由適當溫度之熱處理使其記憶效應達最佳值，作為爾後實際應用之參考。

二、實驗方法

本研究使用高純度 Fe、Mn、Si、Cr 及工業用 $Mn_{23}C_6$、$Mn_{72.8}N_{27.2}$ 母合金，利用真空電弧熔煉技術(Vacuum Arc Re-melting, VAR)，配製 6 種不同成分之 Fe-Mn-Si-Cr--IA 系列合金，包括 Fe-Mn-Si-Cr-C 及 Fe-Mn-Si-Cr-N，Fe-Mn-Si-Cr 之配比則選擇目前所知具有優異記憶效應及抗蝕性之 Fe-30Mn-6Si-5Cr 比例。所熔合金錠置於 1200℃高溫爐中均質化 1.5 小時，再於 1200℃熱輥壓至 6mm 厚度，利用機械加工製成各種規格之試片，再進行 500~900℃、15min 之熱處理後水淬，並將試片切成適當大小。熱輥壓狀態及熱處理後之試片應用掃描式電子顯微鏡(SEM)及高解析穿透式電子顯微鏡(FEG Transmission Electron Microscope)觀察其顯微組織。合金成分應用元素分析儀(Element Analyzer, EA)進行分析，合金顯微結構則應用 X-ray 繞射儀(XRD)分析，實驗採用的靶材為銅靶，特性波長 λ=1.5406Å，掃描速度 4°/min，掃描角度 2θ 為 20°~100°。相變態溫度應用內耗量測儀(Internal friction measuring equipment)進行測試，主要設備包括 SINKU-RIKO IFM-1500M/L-S 測試系統及 NEC-9801VM 電腦處理系統。測量時施加之頻率約為 1Hz，而應變振幅的範圍在 10^{-5}~10^{-4} 間，操作溫度範圍在-150℃~+350℃，加熱冷卻速率設定為 2℃/min. 合金之形狀回復率利用彎曲試驗(Bending test)測試，試片尺寸為 50mm×1mm×1mm。

三、結果與討論

3.1. 合金基本性質

本研究配製熔煉之 Fe-Mn-Si-Cr-Cr 及 Fe-Mn-Si-Cr-N 合金，應用元素分析儀(Element Analyzer EA)分析其化學成分，結果如表 1 所示。由表 1 可知，合金熔煉後所量測分析之化學成分與配製時之標稱成分雖有些許差異，但誤差值不大。以下章節則針對這些合金之基本性質與相關特性進行深入探討與比較。

表1 本研究熔煉配製之6種Fe-Mn-Si-Cr--IA記憶合金之EA成分分析結果(wt%)

合金成分(編號)	Fe	Mn	Si	Cr	C	N
$Fe_{59}Mn_{30}Si_6Cr_5C_{0.05}$(C1)	balanced	30.57	5.86	5.04	0.04	－
$Fe_{59}Mn_{30}Si_6Cr_5C_{0.15}$(C2)	balanced	31.09	5.87	4.87	0.16	－
$Fe_{59}Mn_{30}Si_6Cr_5C_{0.25}$(C3)	balanced	30.17	5.99	4.88	0.23	－
$Fe_{59}Mn_{30}Si_6Cr_5N_{0.05}$(N1)	balanced	30.59	5.87	4.94	－	0.05
$Fe_{59}Mn_{30}Si_6Cr_5N_{0.15}$(N2)	balanced	30.10	5.77	5.12	－	0.14
$Fe_{59}Mn_{30}Si_6Cr_5N_{0.25}$(N3)	balanced	30.16	6.25	5.01	－	0.24

圖 1(a)及(b)分別顯示 **$Fe_{59}Mn_{30}Si_6Cr_5C_{0.15}$** 合金於熱輥壓狀態之內耗及頻率對溫度之相關曲線圖。由內耗曲線圖中發現，加熱與冷卻過程分別在-23℃及 219℃出現內耗峰，這些內耗峰係因為麻田散體相變態所產生，故藉由內耗量測可以確定其相變態溫度。圖 1 中顯示 **$Fe_{59}Mn_{30}Si_6Cr_5C_{0.15}$** 合金之 Ms 與 As 溫度約為 27℃與 163℃。值得一提的是，由於 Fe-Mn-Si-Cr 記憶合金之麻田散體相變態屬於非熱彈型(non-thermo-elastic martensitic transformation)，其相變態時未伴隨晶格軟化(lattice softening)現象，故相變態內耗峰不會出現相對應之頻率極小(minimum of frequency)，亦即相對應之剪模數極小，此結果與具有熱彈型麻田散體相變態(thermo-elastic martensitic transformation)之 Ti-Ni 形狀記憶合金不同【10, 11】。其他 $Fe_{59}Mn_{30}Si_6Cr_5$--C 與 $Fe_{59}Mn_{30}Si_6Cr_5$--N 合金之相變態溫度與程序皆與圖 1 相似，故省略之。

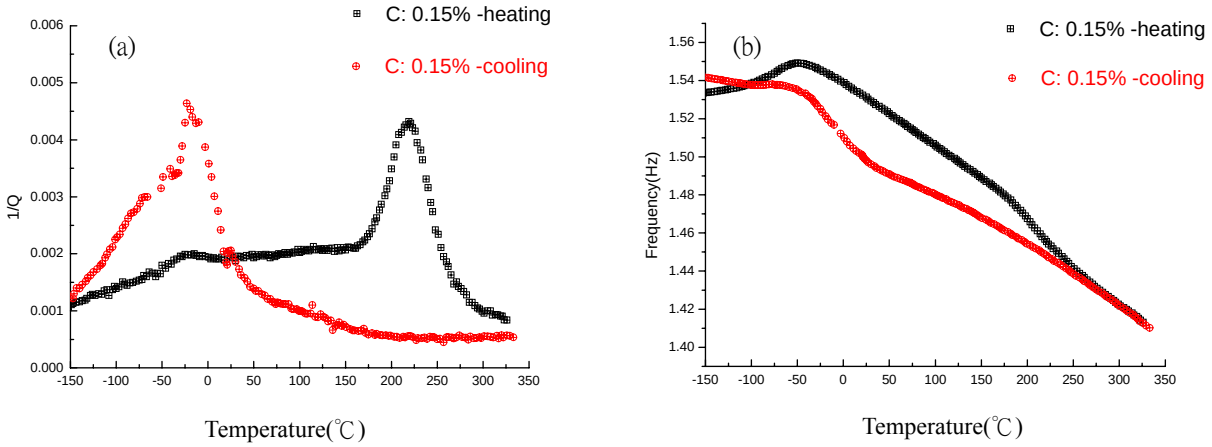

圖 1 $Fe_{59}Mn_{30}Si_6Cr_5C_{0.15}$ 合金熱輥軋狀態下之(a)內耗及(b)頻率對溫度之相關曲線圖

圖 2(a)、(b)分別顯示不同 C、N 含量之 $Fe_{59}Mn_{30}Si_6Cr_5$--C 與 $Fe_{59}Mn_{30}Si_6Cr_5$--N 合金在熱輥軋狀態下之 X-ray 繞射圖，圖中顯示各種合金於室溫下皆主要呈現 γ 沃斯田鐵相，僅些微之 ε 麻田散鐵相存在，此結果與圖 1 之相變態溫度一致，亦即添加微量 C、N 元素會降低 $Fe_{59}Mn_{30}Si_6Cr_5$ 合金之 γ→ε 相變態溫度，故於室溫下主要呈現 γ 相。

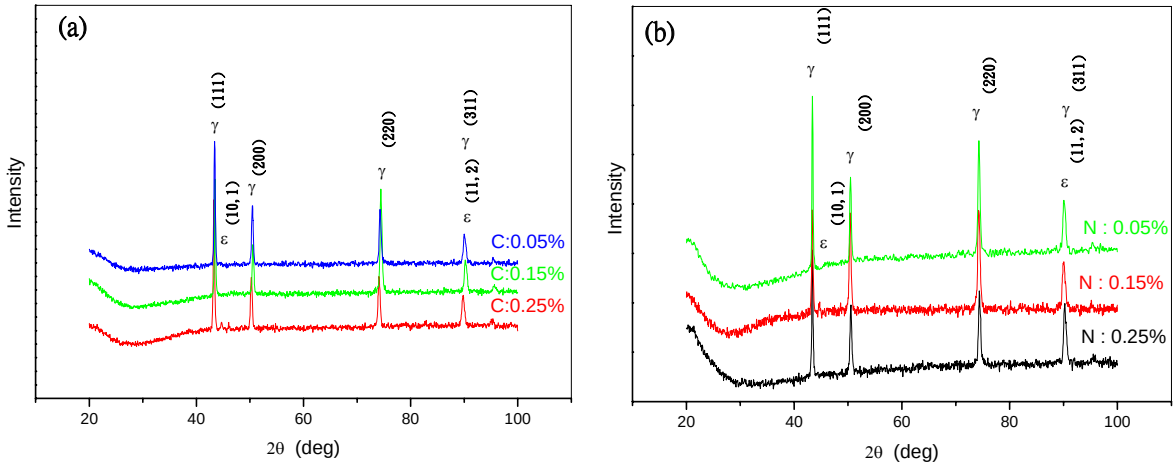

圖 2 Fe-Mn-Si-Cr--IA 記憶合金熱輥軋狀態下之 X-ray 繞射圖
(a) $Fe_{59}Mn_{30}Si_6Cr_5$--C 合金 (b) $Fe_{59}Mn_{30}Si_6Cr_5$--N 合金

圖 3(a-d)分別顯示 $Fe_{59}Mn_{30}Si_6Cr_5C_{0.15}$、$Fe_{59}Mn_{30}Si_6Cr_5C_{0.25}$、$Fe_{59}Mn_{30}Si_6Cr_5N_{0.15}$、$Fe_{59}Mn_{30}Si_6Cr_5N_{0.25}$等四種合金熱輥壓狀態之 SEM 顯微組織。圖中顯示熱輥軋狀態之合金，主要呈現γ相，雖然亦看到少量之ε相。ε相之出現可能是γ→ε相變態溫度已經接近室溫，而於研磨金相試片時在表面產生應力誘發γ→ε相變態所導致，此些結果與圖 1 之相變態溫度及圖 2 之 X-ray 繞射圖所呈現之結果相一致。

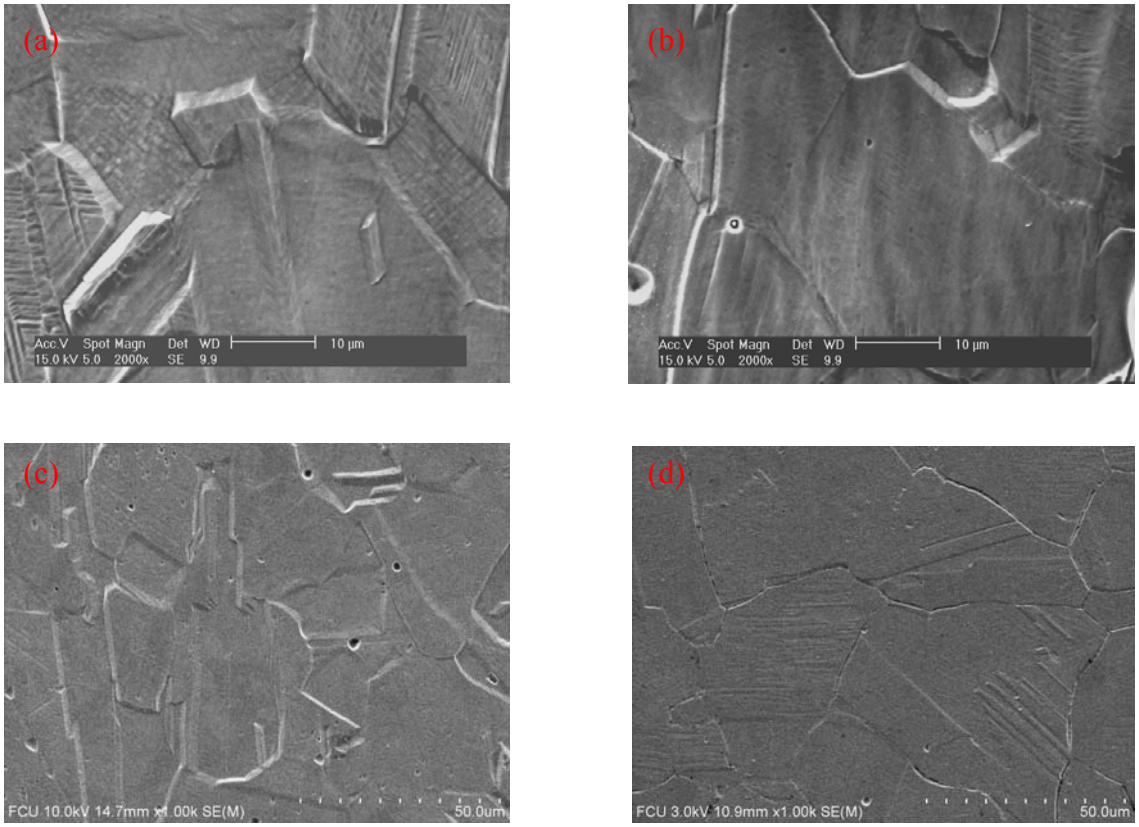

圖 3 Fe-Mn-Si-Cr--IA 記憶合金熱輥軋狀態下之 SEM 顯微組織
(a) $Fe_{59}Mn_{30}Si_6Cr_5C_{0.15}$ (b) $Fe_{59}Mn_{30}Si_6Cr_5C_{0.25}$ (c) $Fe_{59}Mn_{30}Si_6Cr_5N_{0.15}$ (d) $Fe_{59}Mn_{25}Si_6$ $Cr_5N_{0.25}$

3.2. 熱處理效應

圖 4 (a)、(b)分別顯示不同 C、N 含量之 $Fe_{59}Mn_{30}Si_6Cr_5$--C 與 $Fe_{59}Mn_{30}Si_6Cr_5$--N 合金於熱輥軋狀態與經過 500~900℃熱處理後之形狀回復率。另外，未添加 C、N 元素之 $Fe_{59}Mn_{30}Si_6Cr_5$ 合金當作比較對照材。圖中顯示 $Fe_{59}Mn_{30}Si_6Cr_5$ 合金添加 C、N 元素可具有較優異的形狀回復能力，此現象係因為添加 C、N 元素可以提高γ相基地強度，阻止全差排之滑動，且因為γ→ε相變態溫度降低，合金於室溫具有較多γ沃斯田鐵相，形狀記憶變形時產生較多之應力誘發γ→ε相變態，因而於加熱逆變態時具有較優異的形狀回復率。

圖 4 中亦清楚顯現，經過 500~700℃熱處理後可大幅提高其形狀回復率，達 90~92%左右。此結果係因為經過 500~700℃熱處理後，合金逐漸消除熱輥壓後殘留之內應力，並隨著熱處理溫度的提高而產生再結晶，如圖 5 之 SEM 顯微組織所示，這些現象皆會促進γ↔ε正逆相變態之進行，故有效提高形狀記憶能力。但熱處理溫度過高，如 800~900℃，則形狀回復率又降低許多，此乃因為熱處理溫度過高，晶粒快速成長而降低形狀記憶能力【12】。另外，熱處理溫度超過 700℃時，晶界相已經逐漸產生，如圖 6 之 SEM 顯微組織所示。這些晶界相之產生將吸收晶粒內之 C、N 原子，使得γ→ε相變態溫度提高，故於室溫中存在較多的ε麻田散鐵相，ε相之抗蝕性較γ相差，故於圖 5(e)(f)中清楚顯現其腐蝕痕跡。由於過多ε麻田散鐵相之存在，亦使得合金之記憶效應降低許多。

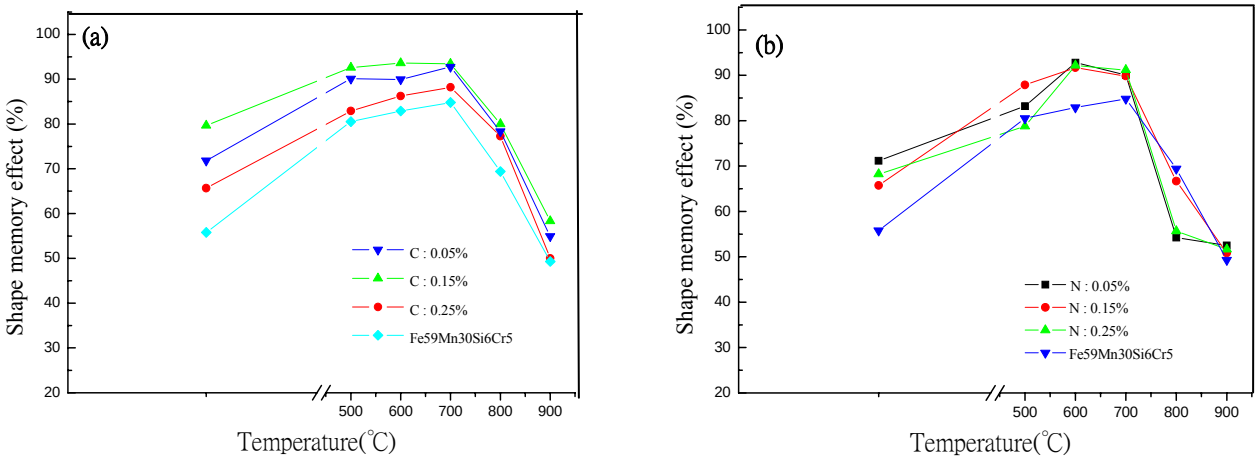

圖 4 Fe-Mn-Si-Cr--IA 記憶合金之形狀回復率與熱處理溫度之關係圖
(a) $Fe_{59}Mn_{30}Si_6Cr_5$--C 合金 (b) $Fe_{59}Mn_{30}Si_6Cr_5$--N 合金

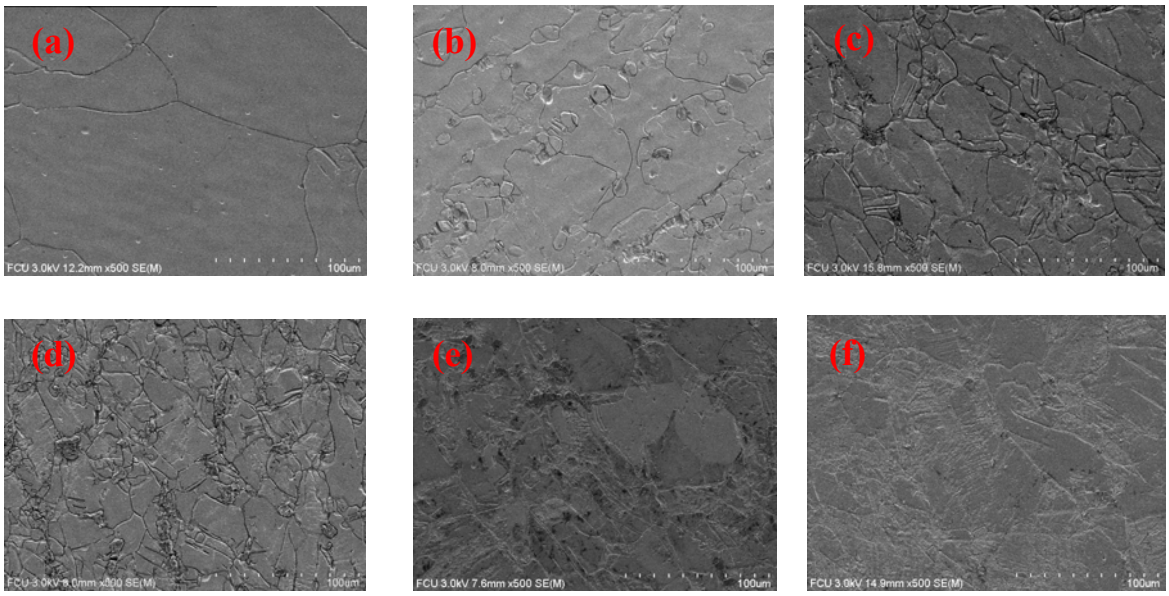

圖 5 $Fe_{59}Mn_{30}Si_6Cr_5C_{0.15}$ 合金經過不同溫度熱處理後之 SEM 顯微組織
(a) 熱輥軋後 (b) 500℃ (c) 600℃ (d) 700℃ (e) 800℃ (f) 900℃

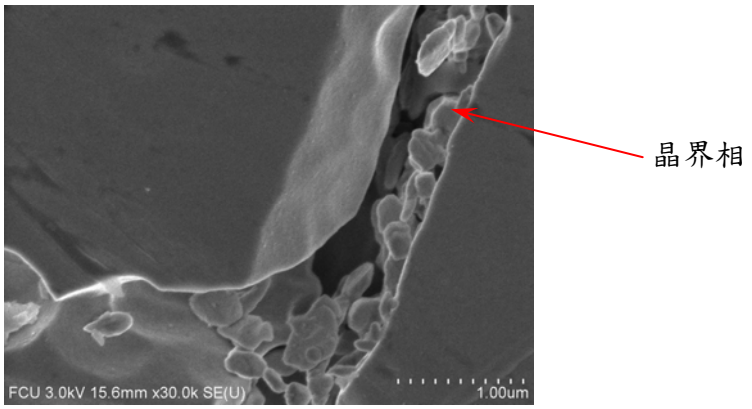

圖6 $Fe_{59}Mn_{30}Si_6Cr_5C_{0.25}$合金經過700℃熱處理後之SEM顯微組織

另外，$Fe_{59}Mn_{30}Si_6Cr_5C_{0.15}$ 合金應用高解析穿透式電子顯微鏡觀察其顯微組織，合金內首次發現雙晶(twin)結構之出現，如圖 7 所示。這些雙晶結構對於形狀記憶效應之影響，將於後續研究中詳細探討。

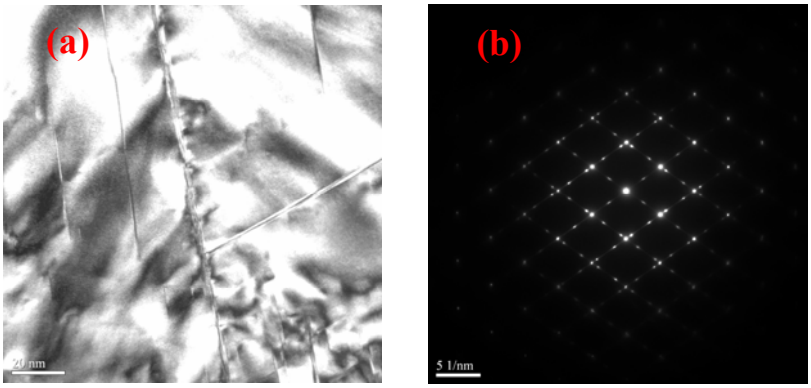

圖 7 $Fe_{59}Mn_{30}Si_6Cr_5C_{0.15}$ 合金應用高解析穿透式電子顯微鏡觀察之明視野及擇區繞射圖

四、成果自評

1. 研究內容與原計畫相符。
2. 達成預期目標概要:人才培育、技術水準之提升。
3. 研究成果的學術與應用價值:高。
4. 研究成果可發表於其他國內外期刊。第一年度計畫之研究成果已被接受發表於 ICPNS-2007 國際學術會議並登載於相關 SCI 期刊。論文題目: Effects of Re Addition on the Fe-Mn-Si-based Shape Memory Alloys
5. 研究結果闡明在Fe-Mn-Si-Cr形狀記憶合金中添加間隙型元素C及N，因可強化沃斯田體相，進而有效提昇其形狀記憶效應。C及N元素添加量約為0.1~0.2wt%時可呈現最佳記憶效應。Fe-Mn-Si-Cr--IA形狀記憶合金於熱輥壓狀態，因合金內部存有過多差排，其記憶效應未達60%，經過500~700℃之熱處理後，熱輥壓殘留之內應力逐漸消除並產生再結晶現象，因而大幅提高其形狀回復率至90~92%。但當熱處理溫度高於800℃時，晶粒快速成長，且由於晶界相析出與合金內部存有較多的ε麻田散鐵相，因而形狀回復率降低許多。

參考文獻

【1】R. Oshima, S. Sugimoto, M. Sugiyama, T.Hamada and F. E. Fujita, Trans. JIM, 26(1985)523.

【2】T. Sohmura, R. Oshima and F.E.Fujita, Scripta Metall., 14(1980)855.

【3】徐祖耀、江伯鴻等著，2000，"形狀記憶材料"，第四章，上海交通大學出版社出版.

【4】Y. N. Koval, V. V. Kokorin and L. G. Khandros, Phys. Met. Metall., 48(1981)162.

【5】T. Maki, K. Kobayashi, M. Minato and I. Tamura, Scripta Metall., 18(1984)1105.

【6】S. Kajiwara, Trans. JIM, 26(1985)595.

【7】A. Sato, E. Chishima, K. Soma and T. Mori, Acta Metall., 30(1982)1177.

【8】B. Jiang, X. Qi, S. Yang, W. Zhou, and T.Y.Hsu, Acta Mater., 46(1996)501.

【9】Murakami M., Otsuka H., Suzuki G., Matsuda S., Proc. ICOMAT-86, Jpn. Inst. Metals,1987,985

【10】S.K. Wu, H.C. Lin and T.S. Chou, Acta Metall., 38(1990)95.

【11】H.C. Lin, S.K. Wu, T.S. Chou and H.P. Kao, Acta Metall. Mater., 39(1991)2069.

【12】S. Tan, Y. Lao, S. Yang, Scripta Metall,Mater., 25(1991)2613.

The 2nd INTERNATIONAL SYMPOSIUM ON FUNCTIONAL MATERIALS (ISFM, 2007) 與會報告書

報告人：林新智　教授

國立台灣大學　材料科學與工程學研究所

中華民國九十六年五月二十五日

（一）參加會議經過

本次會議於民國九十六年五月十六日至五月十九日，在中國大陸杭州市之 HNA Resort Huagang Hotel 舉行，由中國大陸之浙江大學(Zhejiang University)主辦，新加坡國立大學(National Singapore University, NSU)、北京有色金屬研究總院(General Research Institute for Non-ferrous Metals, GRINM)等協辦，是國際上相當重要的功能性材料國際研討會。

本次大會之與會人員大約有 200 人，主要來自中國大陸、新加坡、中華民國、日本、香港、韓國、澳洲、伊朗等國家之學者專家。我國與會者除筆者外，尚有國立台灣大學材料科學與工程學系的楊哲人教授、二位博士生，國立中正大學的張文成教授，逢甲大學的陳世堃教授、一位博士生，國立成功大學電機系的教授與多位研究生等等。本次研討會論文約有 280 篇左右，主要在四個會場舉行，論文發表之主題包括形狀記憶合金、儲能材料、鐵磁材料、鐵磁薄膜、壓電材料、奈米材料以及機能性材料的應用等。本次會議筆者有一篇口頭論文發表(Invited Speaker)，題目為 ” The stress relaxation of a $Fe_{59}Mn_{30}Si_6Cr_5$ shape memory alloy” (附於本報告(五)與會論文內)，具高度學術應用價值，研究成果頗受重視，於會中獲熱烈討論。本次研討會每天由早上 8:30~12:30，下午 13:30~17:50 進行 Oral 與 Poster 論文之發表，時程上相當緊湊。

（二）與會心得

筆者參與此次會議，除發表論文外，並擔任形狀記憶合金之Session Chair，且細心聆聽各場次的演講，與各論文發表者在會中及會後進行討論與交換心得。總括而言，筆者參與此次會議有如下心得：

（1）本次研討會之議題，主要包括形狀記憶材料及應用，儲能材料，鐵磁材料及應用，及其他各種功能性材料，例如壓電材料、奈米材料、薄膜材料、光電材料等。形狀記憶合金之論文發表仍以鈦鎳基記憶合金為主，作者主要來自台灣、韓國、中國大陸、日本、香港等，研究題目包括鈦鎳基形狀記憶合金之合金設計、熱機處理效應以及應用開發等。至於鐵基形狀記憶合金之相關研究不多，但已經引起相關研究學者之關注。

（2）研討會的280篇左右論文中，以中國大陸及日本之論文數量最多，我國約10篇，其餘為澳洲、新加坡、香港、韓國、伊朗等國家。本次研討會有許多在形狀記憶合金領域中相當知名的學者與會，例如日本築波大學的S. Miyazaki教授、澳洲西澳大利亞大學的Y.N. Liu教授及韓國慶尚大學的T.H. Nam教授，故本次研討會參與之國家及學者眾多，所展現之研究水準普遍均高且內容相當廣泛。

（3）由研討會發表論文中顯示，奈米技術及薄膜製程之研究正快速的成長，研究議題包括薄膜電池、記憶合金薄膜、有機/無機材料薄膜、奈米碳管、微細晶粒等，在這次研討會中已有相當多的論文報導相關研究，顯見未來功能性材料必朝向輕薄短小之方向發展。

筆者主要的研究領域為形狀記憶合金與薄膜電池，經由參與本次研討會讓筆者可直接和國際上其他研究形狀記憶合金與薄膜電池之學者交流，因此可快速瞭解國際上其他學者在此些領域中的最新研究方向和結果。因此藉由參加本屆功能性材料國際學術研討會，相信對於筆者爾後之研究具有相當高的助益及啟發作用。第三屆功能性材料國際研討會將在韓國舉行。

（三）攜回資料名稱及內容

1. 本次研討會之 Conference Program & Abstract Book 一本。

2. 本次研討會廠商攤位展示之型錄一份。

3. 本次應邀發表的論文將於會後出版專書。

（四）誌謝

由衷感謝國科會之經費補助，使此趟學術之旅能順利成行。

（五）與會論文(Invited Speaker)

The stress relaxation of a $Fe_{59}Mn_{30}Si_6Cr_5$ shape memory alloy

H.C. Lin[*1], K.M. Lin[2], T.P. Wang[2], C.Y. Chung[2]
[1]Department of Materials Science and Engineering, National Taiwan University, Taipei, TAIWAN
[2]Department of Materials Science and Engineering, Feng Chia University, Taichung, TAIWAN

Abstract

The relaxation phenomena arising from both the static-constrained stress and the cyclic variation of atmospheric temperature of $Fe_{59}Mn_{30}Si_6Cr_5$ shape memory alloy were studied. Experimental results show that the relaxation amount decreases with increasing initial compressive loading. The cyclic variation of atmospheric temperature has a smaller effect on the relaxation than the static-constrained stress does. The relaxation phenomenon is more obvious both in the earlier cycles and at higher cyclic heating temperatures. The static-constrained stress relaxation is ascribed to the combination and rearrangement of the stress-induced thin platelets of ε martensite. The contribution of cyclic heating on the stress relaxation originates from the formation of new-oriented ε martensite. The ε ↔ γ transformation, thermal stress and shape-recovery stress during the thermal cycling are considered to have significant influences on the formation of new-oriented ε martensite.
Keywords: $Fe_{59}Mn_{30}Si_6Cr_5$ shape memory alloy, compressive stress relaxation, thermal cycling

[*] Corresponding author: Department of Mater. Sci. & Eng., National Taiwan University, 1 Roosevelt Rd. Sec. 4, Taipei 106, TAIWAN; Fax: 886-2-2363-4562; E-mail: hclinntu@ntu.edu.tw

Introduction

In light of their low cost and excellent workability, the Fe-based shape memory alloys, which are composed of Fe-Mn-Si compositions, have attracted much attention recently. For example, the Fe-Mn-Si alloys, which contain 28 to 34 wt% Mn and 4 to 6.5 wt% Si, exhibit a nearly perfect shape memory effect (SME) [1-4]. The addition of Cr to the Fe-Mn-Si alloys improves their SME and corrosion resistance [5, 6]. In contrast to the TiNi and Cu-based shape memory alloys, the Fe-Mn-Si-Cr alloys exhibit a non-thermoelastic martensitic transformation. Their SME arises from the reverse transformation of stress-induced ε martensite (HCP structure) into γ parent austenite (FCC structure) upon heating [1]. In the past decade, extensive studies of the Fe-Mn-Si-Cr alloys were made focusing on the transformation behavior [1, 7-9], physical properties [7-10], effects of thermo-mechanical training [11-14] and composition dependence of SME and corrosion resistance [5, 15-21]. Also, effort is made to increase the use of these alloys, especially the "heat-to-shrink" pipe coupling [22]. The fitting technique by using these alloys is a brand-new method to connect engineering pipes. It exhibits much merit than conventional welding and can be widely applied in various engineering fields. However, some problems of Fe-Mn-Si-Cr shape memory alloys should still be investigated and resolved, such as, the stress relaxation phenomena due to the long-time sustaining of constrained stress and cyclic variation of atmospheric temperature. These features will reduce the using life of the fitting pipes and impede their applications. Hence, the understanding of the stress relaxation phenomena of Fe-Mn-Si-Cr alloys is quite important. In the present study, we aim to investigate systematically the stress relaxation by simulating the compressive stress state in the application of pipe fitting. The relaxation phenomena arising from both the long-time sustaining of constrained stress and the cyclic variation of atmospheric temperature are studied. Meanwhile, the variation of microstructures during the stress relaxation will also be discussed.

Experimental procedures

A vacuum melting technique was employed to prepare the $Fe_{59}Mn_{30}Si_6Cr_5$ (wt%) alloy. The as-cast ingot was homogenized at 1200℃ for 24 hrs, hot-rolled at 1200℃ into 35mm-thickness plate and then annealed at 1200℃ for 1.5 hrs. Specimens with dimensions of Φ10 mm×L15 mm were carefully cut from this plate by using a CNC wire electro-discharge machine. The experiments of stress relaxation were carried out on a multi-functional MTS tester equipped with a heating furnace. During the stress relaxation with cyclic variation of atmospheric temperature, the specimen was set to sustain a constant strain and subjected to the repetition of temperature variation, 1 hour at room temperature, followed by a subsequent heating to a set high temperature for 10 minutes and then cooled to room temperature again. The recording of experimental data is completely automatic; calculation and plotting points for the stress-strain curves were carried out by a digit computer. Thus the results with a rather good resolution can be obtained. The XRD analysis was carried out at room temperature with the Philips PW1710 X-ray diffractometer under the conditions of Cu Kα radiation, 30 kV tube voltage, and 20 mA current. TEM specimens were prepared by jet electro-polishing at -25℃ with an electrolyte consisting of 3% $HClO_4$ and 97% C_2H_5OH by volume. TEM observation was carried out by using a JEOL-1200 EX microscope at an operating voltage of 120 kV.

Figure 1 shows the schematic diagram of the stress relaxation. The initial stress (σ_o) decreases rapidly in region I, and then gradually approaches to a relaxation limit

(σ_e) in region II. The amount of stress relaxation is defined as Equation (1).

$$\text{Relaxation (\%)} = \frac{\sigma_o - \sigma_e}{\sigma_o} \times 100\% \qquad (1)$$

Results and discussion

The microstructure at room temperature for $Fe_{59}Mn_{30}Si_6Cr_5$ alloy

Figure 2(a-b) shows the XRD pattern and TEM observation at room temperature for the as-annealed $Fe_{59}Mn_{30}Si_6Cr_5$ alloy. The Ms and As temperatures for this alloy are around 50~60℃ and 140~150℃ [23], respectively. Meanwhile, its Mf temperature is clarified to be below 0℃, although no definite point has been reported. Hence, the γ and ε phases coexist within the alloy at room temperature, as presented in the XRD patterns of Figure 2(a). The coexistence of γ and ε phases within the alloy can also be clearly observed in the TEM observation in Figure 2(b) for the $Fe_{59}Mn_{30}Si_6Cr_5$ specimen.

The phenomena of static-constrained and thermal-cycled stress relaxation

Figure 3 shows the compressive load versus strain for the $Fe_{59}Mn_{30}Si_6Cr_5$ alloy. It is known that the recoverable strain of the polycrystalline $Fe_{59}Mn_{30}Si_6Cr_5$ alloy is about 2~4%. Hence, the constrained strains for the experiments of stress relaxation are set to be in the range of 2~4%, as indicated by a, b, and c in Figure 3. The compressive loads, engineering stresses and strains for these points are presented in Table 1. Meanwhile, the elastic and plastic deformations are found to occur simultaneously in the stress region of a-b-c. The plastic deformation can be introduced by both stress-induced martensitic transformation and dislocation movement.

As mentioned in Section 1, the relaxation phenomena may arise from both the static-constrained stress relaxation (with long-time sustaining of constrained stress) and thermal-cycled stress relaxation (with constrained stress and cyclic variation of atmospheric temperature). Figure 4 (a-b) shows the static-constrained stress relaxation curve with an initial 3000kgf loading at room temperature, and the thermal-cycled stress relaxation curve with an initial 3000kgf loading and 6 times of cyclic heating to 260℃, respectively, for the $Fe_{59}Mn_{30}Si_6Cr_5$ alloy. Figure 4(a) shows a typical curve of static-constrained stress relaxation, namely, the initial stress decreases rapidly and then gradually approaches to a relaxation limit. As shown in Figure 4(a), the limit of static-constrained stress relaxation is about 11.5% for the 3000kgf loading. In Figure 4(b), the thermal-cycled stress relaxation can be divided into two stages. In the first stage, the stress relaxation is mainly contributed from the static-constrained relaxation, which is related to the initial loading. As one can see in Figure 4(a), the static-constrained stress relaxation will complete more than 90% within 30 minutes. Therefore, in stage 2, the stress relaxation is mainly contributed from the effect of cyclic variation of atmospheric temperature, although the relaxation value is small and is related to the cyclic heating temperature and cyclic number. In the real application of pipe coupling, both long-time sustaining of constrained stress and cyclic variation of atmospheric temperature must occur at the same time. Hence, the following part of this paper will mainly discuss the phenomena of thermal-cycled stress relaxation of the $Fe_{59}Mn_{30}Si_6Cr_5$ alloy, which involves simultaneously both contributions of static-constrained stress and cyclic variation of atmospheric temperature.

The effect of initial loading and cyclic heating temperature

Figure 5(a-c) shows the cumulative relaxation at various initial loadings versus cyclic number with heating temperatures of 170℃, 260℃ and 360℃, respectively. The 170℃ ~ 360℃, being around and slightly above the ε → γ transformation temperatures, are selected as the heating temperatures in this study. In Figure 5(a-c), one can find that the cumulative relaxation decreases with increasing initial loadings, namely, 3000kgf < 2750kgf < 2500kgf. This feature can be explained as below. As presented in Table 1, the engineering strains under the loading of 3000kgf, 2750kgf and 2500kgf are 3.9%, 3.0% and 2.4%, respectively. Figure 3 also indicates that the ratio of elastic strain / plastic strain under higher loading is smaller than that under lower loading. Hence, less amount of elastic strain under higher loading will be transferred to plastic strain by internal accommodation during the stress relaxation. These accommodation mechanisms may involve the vacancy diffusion, newly formation of ε martensite and movement of martensite/austenite interfaces. In Figure 5(a-c), one can also find that the relaxation phenomenon is more obvious in the earlier cycles and then gradually approaches to a saturated value. Besides, there occurs a higher cumulative relaxation at a higher cyclic heating temperature.

To understand the effect of cyclic heating temperature, the net cumulative relaxation versus cyclic number for specimens with 3000kgf loading and cyclic heating temperatures of 170℃, 260℃ and 360℃ are plotted in Figure 6. The net cumulative relaxation is only related to the cyclic variation of atmospheric temperature and is calculated by deducting 11.5% (the static-constrained relaxation at room temperature) from the total cumulative relaxation. As shown in Figure 6, the net cyclic relaxation with 6 times of thermal cycling is only 5.2% at a heating temperature of 360℃, and even less than 2.1% at 260℃ and 170℃. This indicates that the cyclic variation of atmospheric temperature has a smaller effect on the relaxation than the static-constrained stress.

TEM analysis of microstructure

Figure 7 (a-b) shows the TEM bright field image and SADP, respectively, of the specimen subjected to a compressive loading of 3000kgf at room temperature. As can be seen in Figure 7 (a), many dense and thin platelets of ε martensite appear within the deformed specimen. Based on the analysis of SADP in Figure 7 (b), these thin platelets of ε martensite exhibit a HCP structure. Figure 8 shows the TEM bright field image of the same specimen as Figure 7, but now it has been subjected to a long-time sustaining of constrained loading. As compared to Figure 7(a), the thin platelets of ε martensite have accommodatingly combined to be thicker ones after the stress relaxation. This indicates that the static-constrained stress relaxation may be ascribed to the combination of stress-induced thin platelets of ε martensite. Meanwhile, the platelets of ε martensite will also rearrange to accommodate the constrained loading, and hence the constrained stress is reduced after a long-time sustaining.

Figure 9 (a-c) shows the TEM bright field images for the specimens subjected to an initial 3000kgf loading at room temperature, being kept the strain and then a heating cycle to 170℃, 260℃ and 360℃ for 10 minutes, respectively. As clearly shown in Figure 9(b-c), in addition to the preferential platelets of ε martensite, there appears other groups of ε martensite with different orientations. The more the thermal cycling, the more quantity of the other groups of ε martensite, as shown in Figure 10 for the same specimens as Figure 9 (a-c), but now with 6 times of thermal cycling. These TEM observations can demonstrate that the effect of cyclic heating on the stress relaxation originates mainly from the formation of new-oriented ε martensite.

This feature is believed to be related to the reverse transformation of ε → γ during heating and the forward transformation of γ → ε during the following cooling process. Meanwhile, the thermal stress and shape-recovery stress under the fixed constrained strain during the heating process will also be expected to enhance the formation of new-oriented ε martensite. At a lower cyclic heating temperature of 170℃, only a small part of ε → γ transformation can occur during the heating process. Hence, no obvious new-oriented ε martensite can be observed after the cyclic heating, as shown in Figures 9(a) and 10(a). It is worthy to mention that the net relaxation amount per cycle decreases gradually with increasing cyclic number, as shown in Figure 6. This indicates that the formation rate of new-oriented ε martensite will decrease with increasing cyclic number. This feature is reasonable because the formation of new-oriented ε martensite will be more difficult in the later thermal cycles.

Conclusions

The stress relaxation of $Fe_{59}Mn_{30}Si_6Cr_5$ shape memory alloy was studied by using a compressive test. The important conclusions are as follows:

1. At higher initial loading, less amount of elastic strain will be transferred to plastic strain by internal accommodation. Hence, the relaxation amount decreases with increasing initial loading.

2. The cyclic variation of atmospheric temperature has a smaller effect on the relaxation than the static-constrained stress does. There occurs a higher amount of relaxation at a higher cyclic heating temperature. Meanwhile, the relaxation phenomenon is more obvious in the earlier cycles and then gradually approaches to a saturated value.

3. The static-constrained stress relaxation is ascribed to the combination of stress-induced thin platelets of ε martensite. Meanwhile, the platelets of ε martensite will also rearrange to accommodate the constrained loading, and hence the constrained stress is reduced.

4. The effect of cyclic heating on the stress relaxation originates from the formation of new-oriented ε martensite. The ε ↔ γ transformation, thermal stress and shape-recovery stress during the thermal cycling are considered to have significant influences on the formation of new-oriented ε martensite.

Acknowledgment

The authors are pleased to acknowledge the financial support of this research by the National Science Council (NSC), Republic of China, under Grant No. NSC 93-2216-E-002-025.

References

[1] A. Sato, E.Chishima, K. Soma and T. Mori; Acta Metall. 30 (1982) 1177.

[2] A. Sato, E.Chishima, Y. Yamaji and T. Mori; Acta Metall. 32 (1984) 539.

[3] A. Sato, K. Soma, E.Chishima, and T. Mori; J. Physique, (1982) C4-797.

[4] M. Murakami, H. Otsuka, H. Suzuki and S. Matsuda, Trans. ISIJ 27 (1987) B-88.

[5] X.X. Wang and L.C. Zhao, Scripta Metall. Mater. 26 (1992) 1451.
[6] T. Moriya et al., Bulletin of JIM (in Japanese), 29 (1990) 367.
[7] H.C. Lin and K.M. Lin; Scripta Metall. Mater. 34 (1996) 343.
[8] H.C. Lin, K.M. Lin and T.S. Chou; Scripta Metall. Mater. 35 (1996) 879.
[9] M. Sade, K.Halter and E. Hornbogen; Z. Metallkd. 79 (1988) 487.
[10] A. Sato, Y.Yamaji and T.Mori; Acta Metall. 34 (1986) 287.
[11] K. Tsuzaki, M. Ikegami, Y. Tomota and T. Maki, ISIJ, 30 (1990) 666.
[12] B.H. Jiang, T. Tadaki, H. Mori and T.Y. Hsu, Mat. Trans. JIM, 38 (1997) 1072, 1078.
[13] B.H. Jiang, X.A. Qi, W.M. Zhou, Z.L. Xi and T.Y. Hsu, Scripta Metall. Mater. 34 (1996) 1437.
[14] R. D. Xia, G. W. Liu, T. Liu, Mater. Lett., 32(1997)131.
[15] T. Maki and I. Tamura; Proc. ICOMAT-86 (1986) 963.
[16] M. Murakami, H. Otsuka, G. Suzuki and M. Masuda; Proc. ICOMAT-86 (1986) 985.
[17] A. Sato, K. Takagaki, S. Horie, M. Kato and T. Mori; Proc. ICOMAT-86 (1986) 979.
[18] O. Soderberg, X.W. Liu, P.G. Yakovenko, K. Ullakko and V.K. Lindroos; Mater. Sci. Eng. A, 273-275(1999) 543.
[19] V. V. Bliznuk, V. G. Gavriljuk, B. D. Shanina, A. A. Konchits, S. P. Kolesnik, Acta Materialia, 51(2003)6095.
[20] J. C. Li, W. Zheng, Q. Jiang, Mater. Lett.,38(1999)275.
[21] H. Kubo, K. Nakamura, S. Farjami and T. Maruyama, Mater. Sci. Eng. A, 378(2004)343.
[22] H. Tanahashi, T. Maruyama and H. Kubo, Trans. Mat. Soc. Japan, 18B (1994) 1149.
[23] W. Zhou, B. Jiang, X. Qi and T.Y. Hsu, Scripta Metall. Mater. 39(1998)1483.

Caption of Tables

Table 1 The engineering stress and strain for the testing specimens with various compressive loads.

Caption of Figures

Figure 1 The schematic diagram of the stress relaxation curve.

Figure 2 (a) XRD pattern and (b) TEM observation at room temperature for the as-annealed $Fe_{59}Mn_{30}Si_6Cr_5$ alloy.

Figure 3 The compressive load versus strain for the $Fe_{59}Mn_{30}Si_6Cr_5$ alloy.

Figure 4 (a) The static-constrained stress relaxation curve with an initial 3000kgf loading at room temperature, and (b) the thermal-cycled stress relaxation curve with an initial 3000kgf loading and 6 times of cyclic heating to 260℃, for the $Fe_{59}Mn_{30}Si_6Cr_5$ alloy.

Figure 5 The cumulative relaxation at various initial loadings versus cyclic number with heating temperatures of (a) 170℃, (b) 260℃ and (c) 360℃.

Figure 6 The net cumulative cyclic relaxation versus cyclic number for specimens with 3000kgf loading and cyclic heating temperatures of 170℃, 260℃ and 360℃.

Figure 7 (a) TEM bright field image and (b) SADP of the specimen subjected to a compressive loading of 3000kgf at room temperature.

Figure 8 TEM bright field image of the same specimen as Figure 7, but now it has been subjected to a long-time sustaining of constrained loading.

Figure 9 TEM bright field images for the specimens subjected to an initial 3000kgf loading at room temperature, being kept the strain and then a heating cycle to (a) 170℃, (b) 260℃ and (c) 360℃.

Figure 10 TEM bright field images of the same specimens as Figure 9 (a-c), but now they have been subjected to 6 times of thermal cycling.

Load (kgf)	Stress(kgf/mm^2)	Strain (%)
2500	31.83	2.4
2700	35.01	3.0
3000	38.20	3.9

Table 1. H.C. Lin et al.

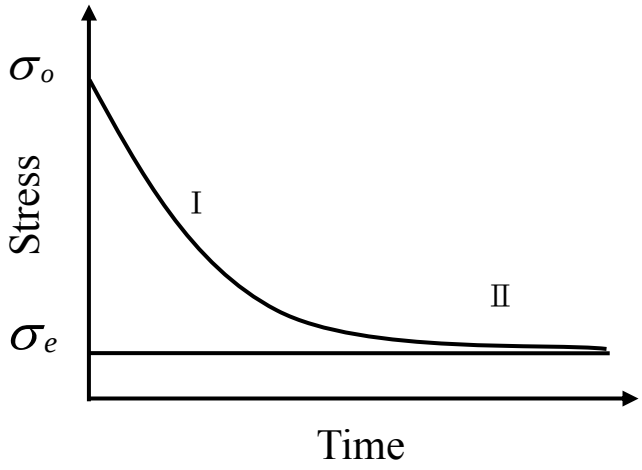

Figure 1 H.C. Lin et al.

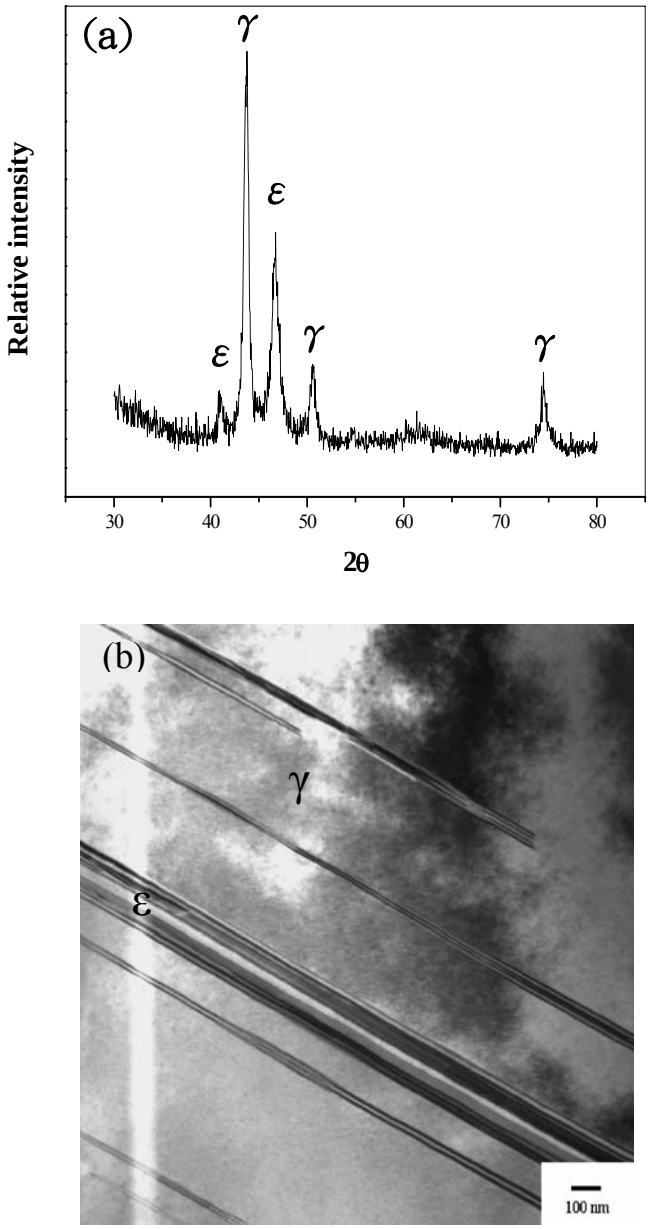

Figure 2 H.C. Lin et al.

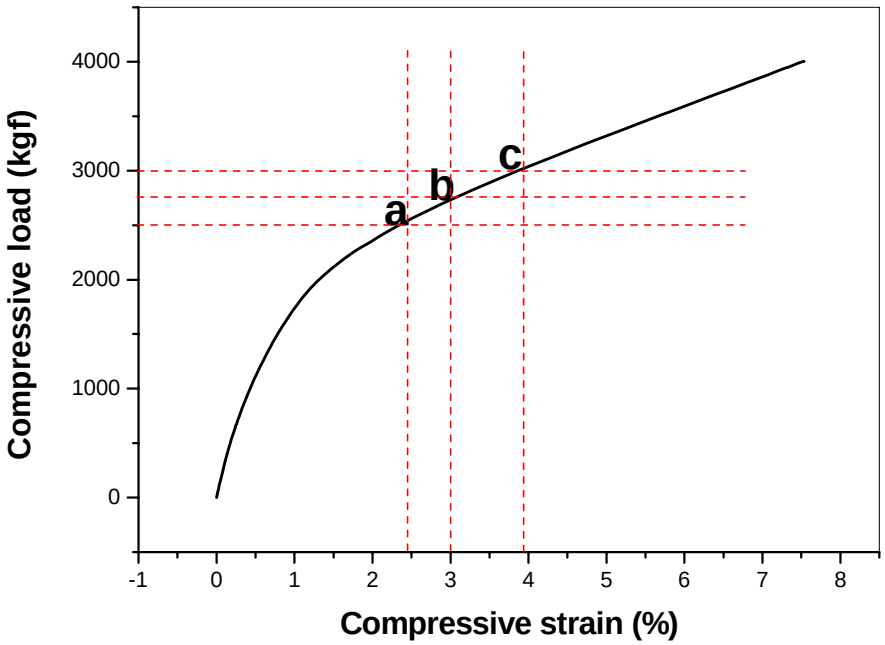

Figure 3 H.C. Lin et al.

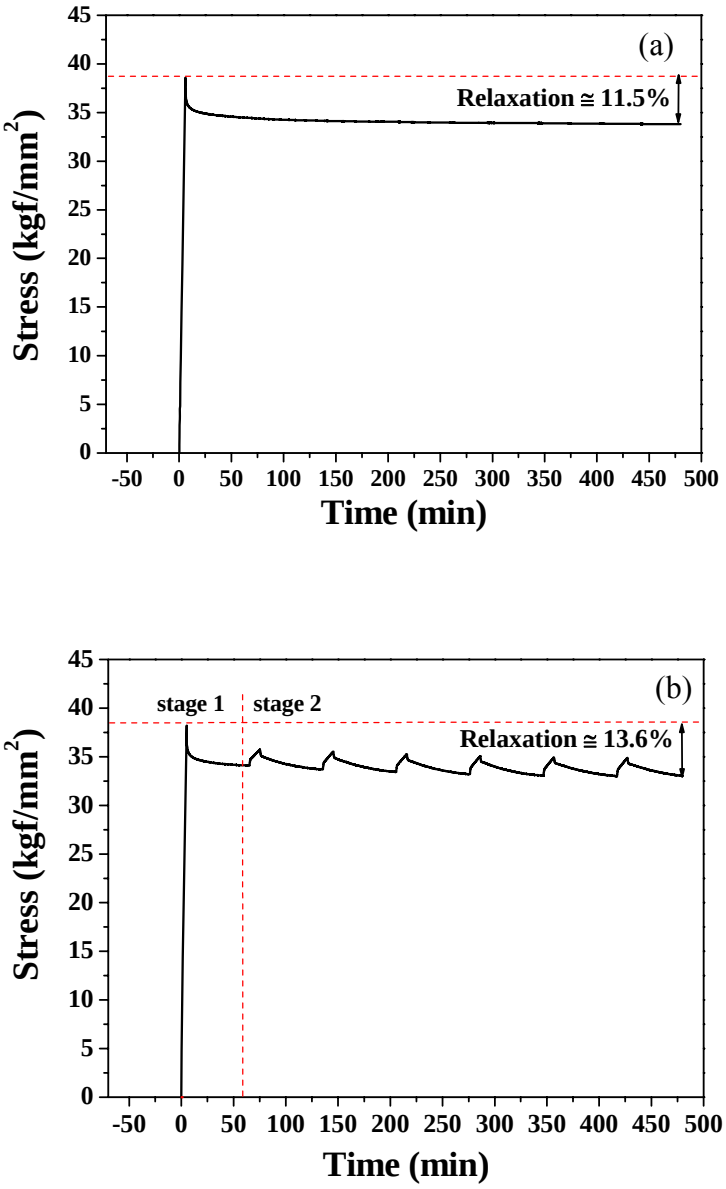

Figure 4 H.C. Lin et al.

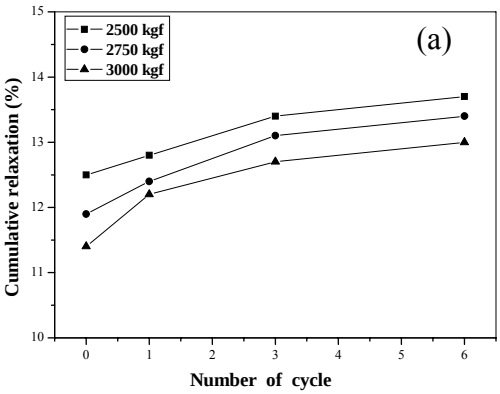

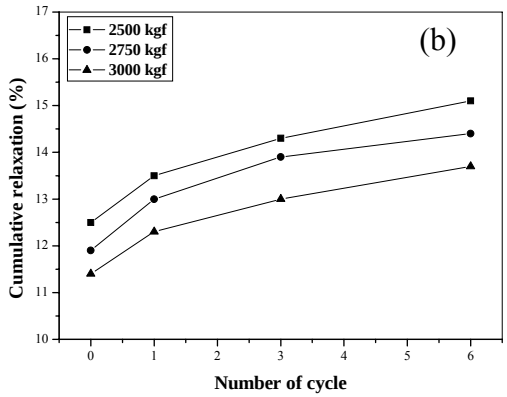

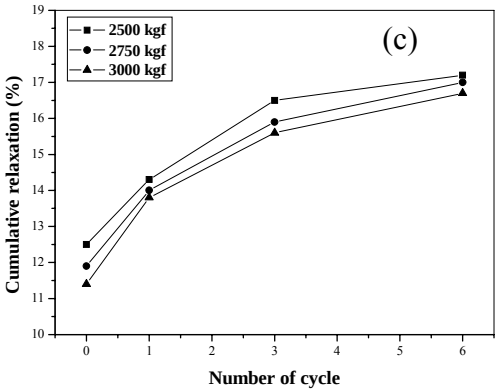

Figure 5. H.C. Lin et al.

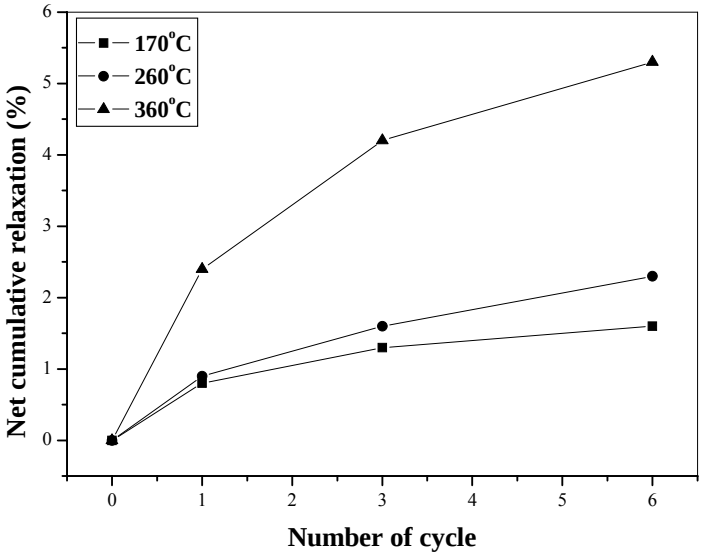

Figure 6. H.C. Lin et al.

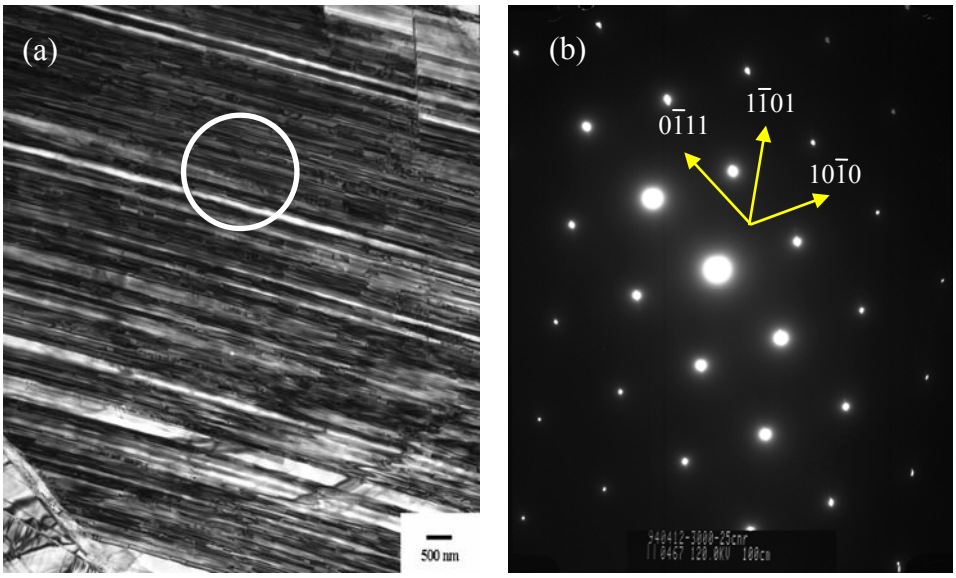

Figure 7 H.C. Lin et al.

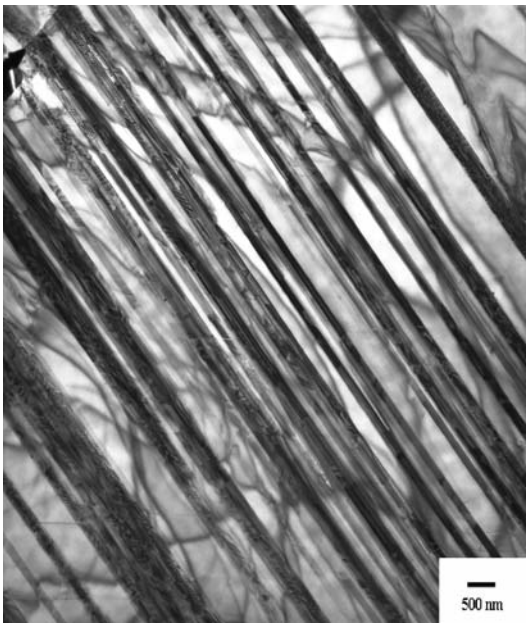

Figure 8 H.C. Lin et al.

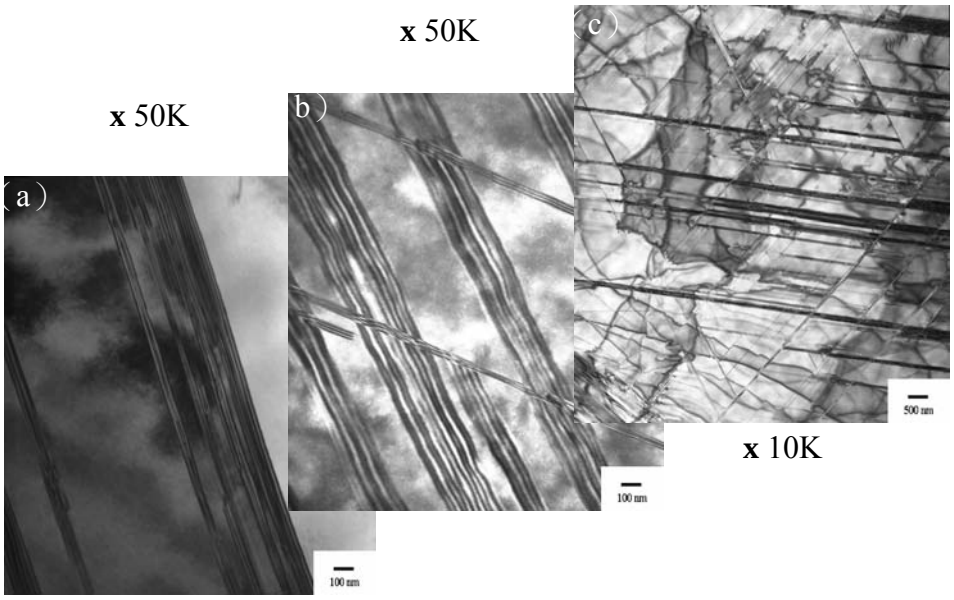

Figure 9. H.C. Lin et al.

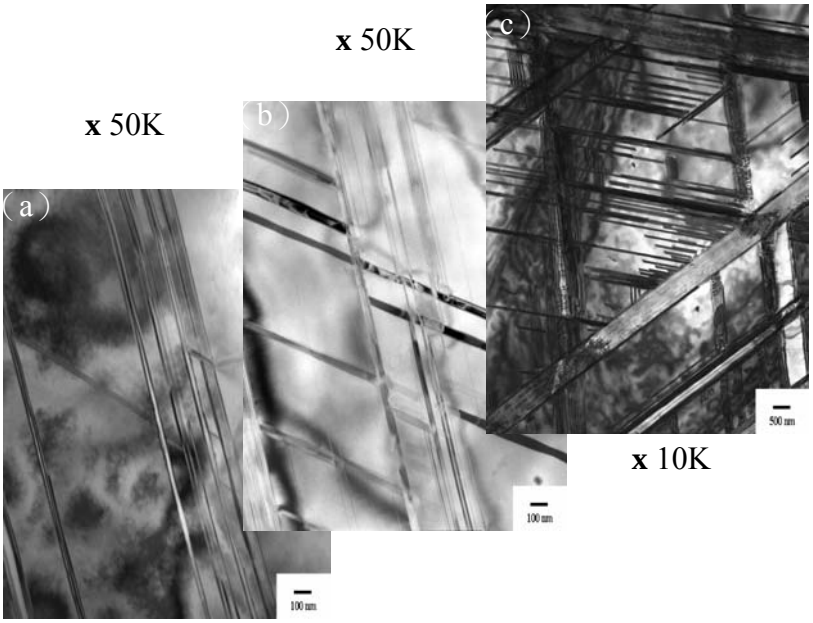

Figure 10 H.C. Lin et al.